Howard Hughes Medical Institute

Published as: *Nature*. 2013 November 14; 503(7475): 262–266.

Feature detection and orientation tuning in the *Drosophila* central complex

Johannes D. Seelig and **Vivek Jayaraman**

Many animals, including insects, are known to use visual landmarks to orient in their environment. In *Drosophila melanogaster*, behavioral genetics studies have identified a higher brain structure called the central complex as being required for the fly's innate responses to vertical visual features[1] and its short- and long-term memory for visual patterns[2–4]. But whether and how neurons of the fly central complex represent visual features is unknown. We used two-photon calcium imaging in head-fixed walking and flying flies to probe visuomotor responses of ring neurons—a class of central complex neurons that have been implicated in landmark-driven spatial memory in walking flies[2,3] and memory for visual patterns in tethered flying flies[5]. We found that dendrites of ring neurons are visually responsive and arranged retinotopically. Ring neuron receptive fields comprise both excitatory and inhibitory subfields, resembling those of simple cells in mammalian primary visual cortex. Ring neurons show strong and, in some cases, direction-selective orientation tuning, with a notable preference for vertically oriented features similar to those that evoke innate responses in flies[1,2]. Visual responses were diminished during flight, but, in contrast with the hypothesized role of the central complex in the control of locomotion[6], not modulated during walking. Taken together, these results suggest that ring neurons represent behaviorally relevant visual features in the fly's environment, enabling downstream central complex circuits to produce appropriate motor commands[6]. More broadly, this study opens the door to mechanistic investigations of circuit computations underlying visually guided action selection in the *Drosophila* central complex.

Flies display a variety of visual pattern- and position-dependent behaviors, including stripe fixation[2], short-term orientation memory[2], pattern learning[4], and place learning[3]. Common to these behaviors is a need to detect and respond to specific features in the insect's visual surroundings. In addition, all these behaviors require the central complex[1–5], a deep brain region that has also been implicated in motor control[6]. We used two-photon calcium imaging in genetically targeted populations of central complex input neurons in behaving flies to investigate their potential visuomotor role. We focused on the dendritic responses of ring neurons—neurons that connect the lateral triangle (LTr) to the ellipsoid body (EB)[7–9] (Fig. 1a), and that have been specifically implicated in visuomotor memory[2,3].

Correspondence and requests for material should be addressed to V.J. (vivek@janelia.hhmi.org).

AUTHOR CONTRIBUTIONS

Both authors designed the study and wrote the manuscript. J.S. carried out the experiments and data analysis.

The authors declare no competing financial interests.

Electron microscopy in the locust has shown that dendrites of ring neuron analogs arborize in specialized structures in the LTr called microglomeruli, where they are contacted by axonal projections from visual areas[10]. Confocal images of the *Drosophila* LTr labeled with GFP under the control of a pan-neuronal driver line, *R57C10*[11], revealed a similar dense microglomerular substructure in the region (Fig. 1b, Supplementary Videos 1–4).

Do LTr microglomeruli respond to visual input? We used two-photon imaging with the calcium indicator GCaMP expressed pan-neuronally to record neural activity in the LTr of head-fixed *Drosophila* placed at the center of a visual arena (Fig. 1c,d). Flies were presented with small bright vertical bars moving horizontally at different elevations, and we recorded LTr calcium transients from multiple planes of focus on one or both sides of the brain in a single experiment (see Methods). Calcium transients showed strong temporal correlations at the spatial scale expected of LTr microglomeruli (Fig. 1e, Supplementary Video 5; Extended Data Fig. 1a). Visual stimuli evoked robust calcium transients in a subset of microglomeruli, but only when the localized stimuli were in specific spatial locations around the fly (Fig. 1f). We computed receptive fields (RFs) for responsive microglomeruli, and found that a majority of RFs are centered in the ipsilateral visual hemifield (Fig. 1g–i, Extended Data Fig. 1b and Methods). Finally, LTr microglomeruli are clustered retinotopically, and principal component analysis based on RF centers suggests that they form a spatial map with axes that are almost parallel to the fly's visual field (Fig. 1j,k, Extended Data Fig. 1c–e).

We next examined the anatomical relationship between the LTr and individual classes of ring neurons that send arbors to the region[8,12]. We studied dendritic arborization patterns of ring neurons targeted by *EB1-GAL4*, which labels R2 ring neurons required for pattern memory[5], and *c232-GAL4*, which labels R3/R4d neurons required for spatial memory[2] (Supplementary Video 1,2 for R3/R4d; Supplementary Video 3,4 for R2). In agreement with past anatomical work[9], different ring neuron classes arborize in specific contiguous parts of the LTr (Extended Data Fig. 2a,b). Each ring neuron in these classes extends dendrites into a single microglomerulus in the LTr, and sends axonal arbors throughout a class-specific ring of the EB (Fig. 2a, Extended Data Fig. 2c–e, see also[7,12]).

To understand whether different types of ring neurons have distinctive visual response properties, we mapped RFs for dendritic microglomeruli of R3/R4d and R2 ring neurons (Extended Data Fig. 3a–c, and Extended Data Fig. 3d–f respectively). We found visual responses in ~7/40 *c232-GAL4*-labeled microglomeruli—corresponding to ~7/20 R4d microglomeruli (Extended Data Fig. 3a)—and ~14/20 of R2 microglomeruli labeled by *EB1-GAL4*. RFs for R2 and R4d neurons cover large parts of the visual field, with highest density near the midline of the ipsilateral visual field (Extended Data Fig. 3g,h). In summary, R4d and R2 microglomeruli appear to have similar visual response properties and overlapping RFs, but with peak sensitivity in different parts of the visual field (Extended Data Fig. 3i–k).

We next probed the fine structure of microglomerular RFs using sparse white noise stimuli (Fig. 2b, see Methods). Reverse correlation of microglomerular responses revealed prominent inhibitory subfields in the RFs (Fig. 2c for R2, Fig. 3a for R4d). The spatial scales of RF structure we observe is within the range for visual features that evoke strong

innate responses in flies, and that are used for visual pattern learning in tethered flies[2,3]. To test the validity of these white-noise-based RFs, we used them to predict responses to novel bar stimuli (Fig. 2d, see Methods). The predicted responses captured much of the temporal and spatial variation in the data (Fig. 2e), with high correlations between estimated and actual responses (Extended Data Fig. 4a,b).

Noting that the RF structure of ring neuron inputs resembles those of simple cells in mammalian primary visual cortex[13], we next asked if these neurons share other response properties. Indeed, when we presented flies with a series of moving oriented bars, we found strong orientation tuning in microglomerular response patterns (Fig. 2f,g). As expected for RF structures with both excitatory and inhibitory lobes, microglomeruli also showed orientation tuning when presented with bars of opposite contrast, i.e., dark bars on a bright background (Extended Data Fig. 5a,b), as are often used in fly behavioral studies[1,2]. Examining orientation tuning across the population of microglomeruli, we observed a strong preference for vertically oriented bars (Fig. 2h and Extended Data Fig. 4h,i for R2, Extended Data Fig. 4c,k,l for R4d, Fig. 2k and Extended Data Fig. 4g,n,o for pan-neuronal line). RFs tuned to vertical orientations are distributed across the visual field (Fig. 2i,j for R2, Extended Data Fig. 4c,d for R4d, Extended Data Fig. 4f for pan-neuronal line). A significant fraction of neurons also shows direction-selectivity (Fig. 2j and Extended Data Fig. 4j for R2, Extended Data Fig. 4e,m for R4d, Fig. 2l, Extended Data Fig. 4p for pan-neuronal line).

Are response properties of ring neuron dendrites stereotyped? We found strong correlations across flies in RF structure for R4d (Fig. 3a–b, Extended Data Fig. 6,8), and R2 (Fig. 3c, Extended Data Fig. 7,8).

Ring neurons and the EB have often been ascribed a role in complex visuomotor tasks[2,3]. We examined the possible motor function of ring neurons by assessing potential correlations between neural activity and locomotion in tethered flies walking on an air-supported ball[14] or flying[15], in darkness or in the presence of a bright stripe moving left or right in front of the fly (Fig. 4a, see also Methods and Supplementary Video 6,7). Although some R3/R4d neurons did show occasional correlations with locomotion when flies walked in the dark, and responses from visually stimulated animals showed occasional modulation during walking, the changes were within the expected variability of visual responses in stationary flies (Fig. 4b–d). Responses were also insensitive to walking direction. Overall, LTr visual responses could be modeled accurately without taking walking state into account (Extended Data Fig. 9a–e and 10). By contrast, responses to visual stimuli were consistently diminished during tethered flight (Fig. 4e,f, Extended Data Fig. 9f–h, Supplementary Video 7), but showed no obvious correlations with flight direction as assessed by differences in wingbeat amplitude envelope. Thus, ring neuron LTr responses were modulated by motor state, but not in a manner consistent with a direct role in motor coordination, and in a markedly different manner than in the optic lobe[15,16].

Behavioral genetics studies in *Drosophila* have suggested that the central complex is required for a wide range of important sensorimotor functions. However, in the absence of physiological recordings from the region in flies, it has been challenging to constrain its role in the diversity of behaviors that it has been implicated in. We studied the visuomotor

responses of ring neurons, which provide input from the LTr to the ellipsoid body of the central complex. Analogous neurons in other insects respond to polarized and unpolarized light[17–19], and to mechanosensory stimulation[20], one of the sensory modalities that we did not explore but that may partly account for unresponsive neurons in our study. We found that R2 and R4d ring neurons are visually responsive, and these responses are not significantly modulated by walking state. Although visual responses are diminished during flight, they do not vary systematically with wingbeat patterns associated with turns. It is possible that outputs of these ring neurons within the EB rings could be more sensitive to motor actions, but our physiological results in their dendrites during behavior are inconsistent with a major role for these ring neurons in motor coordination in the fly. Further, the high degree of stereotypy that we observe in ring neuron receptive field characteristics across flies suggests that, rather than directly performing motor coordination, these neurons likely provide downstream central complex circuits with similar behaviorally relevant visual feature sets on which to base motor decisions. As a striking example, the strong vertical tuning preference we observe in the LTr may partly underlie the tendency of flies to fixate on vertical edges during both flight and walking[1,2,21]. Recent work has suggested that vertical stripe fixation during walking largely relies on a hypothesized position system sensitive to local luminance changes that can operate independently of neural circuits involved in optomotor responses to widefield motion[21,22]. The response properties of R2 and R4D neurons is consistent with a role in such a position system[22].

The retinotopic bias, structure of excitatory and inhibitory subfields, orientation tuning and direction selectivity we see are reminiscent of those seen in calcium imaging studies in simple cells in mammalian visual cortex[13], providing an interesting example of how evolutionarily distant visual systems with different types of eyes nonetheless use similar feature sets to process visual scenes. From Hubel and Wiesel's findings several decades ago[23] to the present, significant progress has been made on identifying neural representations used at different stages in the mammalian visual system. However, mechanisms underlying simple cell responses are not yet fully understood[24]. With its array of genetic tools, *Drosophila melanogaster* may allow us to uncover how spatiotemporal interactions of excitatory and inhibitory inputs might produce similar orientation tuning and direction selectivity in the LTr[25,26]. There is considerable evidence for spatially tuned visual responses in the lobula complex and anterior optic tubercle in other insects[27–30], suggesting that components of ring neuron input response properties may also arise from selective averaging of weaker and more broadly distributed tuning preferences in such areas.

Overall, our findings lay the groundwork for future research into how this genetic model organism's small brain uses feature and pattern information for visual orientation and navigation.

METHODS

Fly stocks

All experiments were performed with female flies, with ages chosen based on expression levels of relevant fluorescent proteins. At least six animals were used for any single condition tested – specific sample sizes are noted for each set of experiments and were

chosen based on the level of variability observed in initial experiments. Flies were randomly picked from their housing vials for all experiments. We used all data that passed a quality threshold based on the observed health of the fly during an experiment and the signal-to-noise ratio of the imaging signal.

Calcium imaging experiments to measure RFs were performed with *UAS-GCaMP3; c232-GAL4*, *UAS-GCaMP3;EB1-GAL4*, and *pJFRC7-20XUAS-GCaMP5.003 (VK00005)/ R57C10-GAL4* flies. We used *pGP-JFRC7-20XUAS-IVS-GCaMP6f 15.693(attP40)/ R57C10-GAL4* flies for pan-neuronal orientation tuning experiments (2–5 days old) and *pGP-JFRC7-20XUAS-IVS-GCaMP6s 15.641 (attP40)/c232-GAL4* for orientation tuning experiments (1–2 weeks old) with dark bars. *c232-GAL4* and *EB1-GAL4* were gifts from M. Heisenberg and T. Lee, respectively.

To label dendrites and axons in different ring neurons, *EB1-GAL4* and *c232-GAL4* were each crossed to *pJFRC67-3XUAS-IVS-Syt-GFP(attP18)*[31,32], *pJFRC118-10XUAS-DenMark*(attP40)[32,33], and *pJFRC119-10XUAS-IVS-myr::TopHat2(VK00005)* (gift of B.D. Pfeiffer, unpublished).

To compare the expression patterns of *EB1-GAL4* and *c232-GAL4* to the pan-neuronal line *R57C10* in the same fly, *EB1-GAL4* and *c232-GAL4* were each crossed to *pJFRC19-13XLexAop2-IVS-myr::GFP (su(Hw)attP8)*[32], *pJFRC21-10XUAS-IVS-mCD8::RFP (attP18)*[32]; *Sco/Cyo; R57C10-LexA::p65 (attP2)*[34].

For stochastic single cell labeling of *EB1-GAL4* and *c232-GAL4* with three colors a “flip-out”-based approach[35] (Nern et al., in preparation) was used. In brief, heat-shock induced expression of FLP recombinase was used to excise FRT-flanked interruption cassettes from UAS reporter constructs carrying HA, V5 and FLAG epitope tags, and stained with epitope-tag specific antibodies. This results in labeling of a subset of the cells in the expression pattern with a stochastic combination of the three labels.

Anatomy: fly dissections, immunohistochemistry and confocal imaging

Confocal stacks were recorded with a 40x or 63x objective on a Zeiss confocal microscope. Dissections and staining were performed as previously described[36,37]. The primary antibody mixture consisted of 1:1000 sheep anti-GFP (AbD Serotec), 1:1000 rabbit anti-DsRed (Clontech), 1:100 rat anti-HA (for Syt/DenMark/HA staining; Roche), and 10% normal donkey serum (Jackson ImmunoResearch) in PBS-TX.

Fly preparation for RF mapping

RF measurements were performed using a preparation described previously[14], but with the behavioral apparatus removed to maximize the fly’s visual field. The fly was briefly anesthetized on ice and transferred to a cold plate held at 4°C. The proboscis of the fly was fixed by either pressing it into the head and fixing it with wax, or by stretching it with a pair of tweezers mounted on a micromanipulator and then fixing it with a mixture of wax and colophony. We additionally removed either the front legs or all legs for RF measurements. The fly was glued to a pin and positioned in the holder using a micromanipulator and fixed in the holder with UV gel[14]. An opening was cut into the head to obtain optical access to the

brain. To stop brain movement due to pulsation of muscle M16, we cut the muscle or the nerves innervating the muscles with dissection needles. The fly holder (including the micromanipulator) was then transferred to the microscope and mounted using magnetic mounts. Flies were dark adapted for 5 to 10 minutes before recordings started.

Fly preparation for imaging during walking

For walking experiments, an air-supported ball was positioned under the fly with a three-axis micromanipulator as described previously[14] and the walking velocity of the fly was monitored using a camera system.

Fly preparation for imaging during tethered flight

For flying fly experiments a holder similar to those described previously[14,15,38] was used. The holder was made out of two pieces of stainless steel shim (thickness 12.7 μm). The shim is cut using a laser mill and then folded into its pyramidal shape. One piece of the holder is glued onto a liquid chamber similar to the one used for walking behavior using epoxy[14]. After removing the front legs of the fly to prevent it from grabbing the holder, the fly is glued to a pin and inserted into the holder with a micromanipulator. The second piece of the holder is then inserted to close the pyramidal shape around the fly's head.

The setup for combined imaging and flight behavior was similar to the one described in[15]. The fly was illuminated with IR light from below. The wing beat of the fly was recorded using a mirror placed beneath the fly and a camera (Basler 602f, operating at 100 or 150 Hz frame rate)[15].

Two-photon imaging

Calcium imaging was performed using a custom-built two photon microscope controlled with ScanImage[39]. Fluorescence was detected using a photomultiplier tube (H7422PA-40, Hamamatsu). We used an Olympus 40x objective (LUMPlanFl/IR, NA 0.8) and typically adjusted the power to below 20 mW at the back aperture of the objective. We imaged at a frame rate of 6.7 Hz. Focal planes were selected based on the anatomy and visual responses of microglomeruli. We focused on microglomeruli because this approach allowed us to distinguish different neurons in a labeled population (such distinctions are difficult to make in the EB, where axons of different neurons arborize in close proximity).

Visual stimulation

LED arena—Visual stimuli were presented using a curved visual display[40] that was covered with a color filter to prevent cross-talk between fluorescence detection and visual stimulation as described[14]. Additionally, to avoid reflections of stimuli from the curved surface of the display, we covered the display with a diffuser (tracing paper). Under such low-contrast conditions, we found that the signal-to-noise ratio (SNR) of calcium responses when stimulated by dark-on-bright-background stimuli (e.g., dark bar on bright surround) was low. This motivated our preference for bright-on-dark-background stimuli, which produced higher SNR calcium responses (comparison in Extended Data Fig. 5).

For RF measurements the display spanned 270° in azimuth and 120° in elevation. The top left and top right corners of the display (three square panels in each corner, each with a size of 30° by 30°) could not be seen by the fly (since they were occluded by the fly holder) and were excluded from the display. For behavioral experiments, a similar but smaller display was used, spanning 210° in azimuth and 90° in elevation.

Flashing dots for RF mapping—Excitatory RFs for *c232-GAL4* and *EB1-GAL4* flies were measured with stationary bright square dots (7.5° by 7.5°) appearing randomly in the visual field of the fly for 1s followed by a dark period of 1s. The measurements were repeated until the entire visual field covered by the display was stimulated once. The display was sampled with a spatial resolution of the stimulus (7.5°). Measurements were performed in 8 blocks of 140s each, presenting a total of 468 stimuli covering the entire display.

Horizontally moving bars for RF mapping—We used bright bars (15° in elevation, 7.5° in azimuth) that moved at a speed of 30 °/s left and right (in azimuthal direction) in the fly's field of view.

Two repetitions with stimulation in one direction were followed by two repetitions of movement in the opposite direction. To map responses over the entire visual field spanned by the display the stimulus was shifted in steps of 15° in elevation from the top most part of the visual display towards the bottom part and the left and right moving stimulation was repeated in each row.

White noise—For white-noise stimulation[37,41] we subdivided the display into squares of 11.25° by 11.25°. Each stimulus frame consisted of 20 randomly selected bright squares while the remaining squares remained dark (in a few trials for one fly we used 30 squares). The stimulus appeared for one second followed by a dark period of one second. We presented 60 frames of random stimuli in a trial of 140 s. For *c232-GAL4* flies we used an average of 33 +/− 20 trials in 7 flies (59, 61, 29, 21, 21, 14, and 26 trials, respectively). For *EB1-GAL4* flies we used an average of 41 +/− 13 trials in 6 flies, (38, 25, 39, 63, 35, and 47 trials, respectively). The color scale (Fig. 2, Extended Data Fig. 8) was adjusted to give equal weight to excitatory and inhibitory subfields (mean set to 0).

To validate white noise based responses we stimulated the fly with bright bars of 56.25 degrees by 18.75 degrees oriented either vertically, horizontally, or rotated by 45 or −45 degrees with respect to the vertical direction. To stimulate the receptive fields of all microglomeruli in an unbiased way, the bar stimuli were presented at a random position on the display and the display was sampled with a resolution of 11.25° in both elevation and azimuth.

Visual stimulation for measuring orientation tuning curves—For orientation tuning curve measurement we used a stimulus that extended across the entire display, from 120° in azimuth for vertical orientation (90°) to 270° azimuth for horizontal orientation. The width of the bar was 15° and it was moved at a speed of 75°/s. The angle was changed incrementally in steps of 11.25° starting with either horizontally or vertically oriented bars for one direction of movement, and then repeated in the opposite direction of movement. To

obtain tuning curves with dark stimuli we inverted the contrast of bright and dark, and removed the diffuser.

Visual stimulation during walking and flying experiments—For walking and flying experiments we used a vertical bright bar spanning 90° in elevation and 15° in azimuth. The bar moved horizontally at a velocity of 15 °/s. The bar stayed stationary for 10 s after moving in one direction for 17 s and then resumed moving in the opposite direction for 17 s.

Data analysis

All data analysis was performed in MATLAB (MathWorks, Inc., Natick, MA). All errors and error bars shown are standard deviation (s.d.). All p-values shown are based on t-tests, unless otherwise noted.

Frame alignment and movement correction—Data recorded using two-photon imaging were aligned in the XY plane on a frame-by-frame basis. Data were thresholded to distinguish arborizations in the lateral triangle from background. All above-threshold pixels were set to the same value. Frames were aligned by cross-correlating each thresholded frame to a single frame at the beginning of the measurement. Multiple trials were aligned by cross-correlation of trial-averaged frames thresholded as above.

Calculation of fluorescence changes—The baseline for calculating ΔF/F was selected by averaging over the 10% of frames with lowest intensity in each trial or by using the baseline at the beginning of the experiment. Due to the low baseline intensity of GCaMP6, background fluorescence was not subtracted in measurements with GCaMP6. Calcium traces recorded from behaving flies were smoothed with a third order Savitzky-Golay filter over 7 frames for comparisons with behavioral data.

ROI selection—For RF measurements in stationary flies, ROIs corresponding to microglomeruli were selected manually in videos of ΔF/F. Overlapping parts of ROIs were excluded from further analysis.

For experiments in behaving flies, ROIs were selected using visually supervised k-means clustering (Extended Data Fig. 10a–d). We used a subset of three trials (2820 frames) for clustering-based selection of ROIs. We then used correlation-based k-means clustering between the calcium traces in all thresholded pixels. The number of clusters was selected based on an estimate of the number of microglomeruli. If not all microglomeruli could be separated into different clusters, the number of clusters was increased in a second run. We then set a threshold to remove clusters that were smaller than a certain number of pixels (60). We additionally removed clusters that had an average cross-correlation value lower than a threshold (0.2). We further split anatomically disconnected regions of the same cluster and again removed those parts that were smaller than a size threshold (30 pixels). In a final check, the remaining ROIs were overlaid with the frames of the calcium video that showed the largest response in this ROI, and ROIs that did not correspond to microglomeruli were removed manually.

RF mapping—RFs were smoothed using a Gaussian filter (4 pixels with a standard deviation of 1 pixel by default; 5 pixels with a standard deviation of 4 pixels for white noise measurements).

For RF measurements (e.g., in Fig. 1), we combined responses to left- and right-moving stimuli (each averaged over two trials). The onset of the calcium response was correlated with the bar's movement into the RF. Due to the size of the RF, a bar moving from the right side of the fly towards the left side entered the RF from the right side and induced a calcium onset starting at the right side of the (excitatory part of the) RF. Similarly, a bar entering the receptive field from the left side induced a calcium onset starting at the left side of the RF. Due to the faster on-response than off-response of GCaMP the onset of the RF was better defined than the offset. To find the center of the excitatory RF measured with moving bars, we defined the RF center as the weighted centroid of the average of responses to thresholded left- and right-moving stimuli (Extended Data Fig. 1 b). This was equivalent to delimiting the RF by its calcium onset response. This procedure made the location of computed RF centers invariant to the kinetics of the calcium indicator.

We used the following parameters to characterize the excitatory parts of RFs measured with single stationary dots (measured at 50% of the maximum ΔF/F response of each RF) (see Extended Data Figure 7c): area, major axis (of an ellipse that has the same normalized second central moments as the region as determined with the MATLAB 'regionprops' function), minor axis, eccentricity, orientation (the angle between the horizontal x axis and the major axis of the ellipse, 0 corresponding to horizontal orientation), retinotopic correlation (the correlation coefficient between the center of the RF, determined as the weighted centroid of the RF area, and the center of the corresponding ROI).

RF display—To display microglomerular RFs, we colored LED arena positions in proportion to the ΔF/F response elicited by the stimulus presented in that position. For moving stimuli, the calcium response in each pixel was determined as the average over all response frames that were recorded while the stimulus was at that position. Calcium responses were interpolated to account for mismatches between frame rates and movement of stimuli. For stimulation with stationary stimuli, the ΔF/F values shown in RF plots correspond to the maximum ΔF/F during the stimulation period. To prevent cross talk between sequentially presented stimulus frames due to the slow decay of the calcium response (which extended beyond stimulus presentation) we only considered the calcium increase and not the calcium decay in assigning ΔF/F values to stimulus frames.

Retinotopy—To assess retinotopy, we calculated the correlation coefficient between microglomerulus centers and centers of their RFs. This was compared to the correlation coefficient obtained after randomly shuffling correspondences.

Additionally, we performed principal component analysis (PCA) on the (x,y) values of RF centers. The first PC gave us the direction of maximum variation of RF centers, which we consider to be the primary retinotopic axis (in the fly's visual field) for the RF population.

Orientation tuning—To measure orientation tuning (Fig. 2), single 15°-wide bars spanning the entire visual display were presented, and their orientation changed in steps of 11.25°. Responses from multiple trials were then averaged, and tuning curves were fit using the sum of two circular Gaussians[42,43].

$$a_1 \cdot e^{-k_1 \cdot (\cos(\theta - \theta_1) - 1)} + a_2 \cdot e^{-k_2 \cdot (\cos(\theta - \theta_2) - 1)},$$

where, a_1 and a_2 are amplitudes, θ_1 and θ_2 are the maximum angles and k_1 and k_2 are width parameters.

The preferred orientation for each microglomerulus was the maximum of its fitted tuning curve.

Orientation selectivity—The orientation selectivity index[44], OSI, was computed as the difference between the response in the preferred direction, $\Delta F/F_{max}$, and the direction orthogonal to it (preferred direction +/− 90°), $\Delta F/F_{ortho}$, normalized by the sum of the responses in the two directions:

$$\mathrm{OSI} = (\Delta F/F_{\max} - \Delta F/F_{\mathrm{ortho}})/(\Delta F/F_{\max} + \Delta F/F_{\mathrm{ortho}}).$$

Direction selectivity—The direction selectivity index[42], DI, was calculated as the difference between responses in the preferred direction, $\Delta F/F_{max}$, and anti-preferred direction (preferred direction+180°), $\Delta F/F_{opposite}$, normalized by their sum:

$$\mathrm{DI} = (\Delta F/F_{\max} - \Delta F/F_{\mathrm{opposite}})/(\Delta F/F_{\max} + \Delta F/F_{\mathrm{opposite}}).$$

The sign of the DI was defined as positive for front-to-back movement and negative for back-to-front movement.

White-noise-based RFs and response predictions—RFs were reconstructed by thresholding calcium traces at 30% ΔF/F and averaging over all frames that induced a response larger than this threshold, weighted by peak calcium response. Only the rising slope of the calcium response was considered. The displayed RFs are the weighted averages of stimulus frames and the mean value (background) is subtracted. Max is the maximum of the weighted average after subtracting the mean value, and min is the minimum of this average. The mean value is set to 0.

To predict responses to oriented bars (Fig. 2), we multiplied the mean-subtracted white-noise-based RF with stimulus values in each pixel and summed over all pixels. We convolved the result with a calcium response function. The amplitude and time constants of the calcium response function were fitted using responses to bars of one orientation and then used in the prediction of responses to the remaining three orientations.

The calcium response function, *crf*, used in predicting responses to oriented stimuli and in the analysis of calcium responses recorded during behavior (see below) is given by

$$crf \sim (1 - (e^{-\frac{(t-t_0)}{t_{on}}})) \cdot (e^{-\frac{(t-t_0)}{t_{off}}}),$$

where t_0 is the onset time, and t_{on} and t_{off}, are the rise and decay times, of the calcium indicator.

Walking behavior analysis—Ball movement was recorded with a sampling rate of 4 kHz and velocities were calculated with a time base of 250 ms. Velocities were then averaged over all velocity values in each two-photon imaging frame. Average velocities were calculated by detecting epochs in which the fly was moving and then averaged over this period. Due to strong walking activity in behaving animals, there were few recordings that allowed us to compare microglomerular responses in walking and stationary conditions (Extended Data Fig. 10e–n).

Flight behavior analysis—The wing angle was detected by first manually identifying the wing hinge in both wings. The wing was then detected by first subtracting the background recorded while the fly was not flying, smoothing with a mean filter, and setting a threshold for detecting the wings in two ROIs surrounding the wings. The wing angle was then defined as the angle between the wing hinge and the tip of the wing. Flight was typically intermittent (Extended Data Fig. 10o,p).

Model for fitting responses of visual microglomeruli during behavior—For describing the calcium responses of visual microglomeruli during walking behavior we fitted the responses with a model consisting of a single excitatory and inhibitory Gaussian function. Model fitting was only performed for microglomeruli that responded with a single peak during one passage of the stimulus on the display, not for bilateral receptive fields. The initial position of each Gaussian, the (common) standard deviation and the amplitude were used as fit parameters. Since the inhibitory responses could not be directly observed in our calcium signals, we set all negative values to zero.

$$rf \sim (e^{-(x-x_0)^2/(2\sigma_x{}^2)} - e^{-(x-x_1)^2/(2\sigma_x{}^2)}), rf = 0 \text{if} rf < 0,$$

where, x_0 and x_1 are the location of the excitatory and inhibitory receptive fields, respectively, and σ_x is the width of the receptive field. The calcium signal *s* (ΔF/F) was then modeled as the convolution of the receptive field with the calcium response function, *crf*, and a constant offset, *bg*,

$$s \sim crf \otimes rf + bg.$$

Since the response in flying flies depended on the state of the fly we used a model for the receptive field that additionally included the left and right wing angles as parameters

$$rf_{flying} \sim behavior \cdot (e^{-(x-x_0)^2/(2\sigma_x{}^2)} - e^{-(x-x_1)^2/(2\sigma_x{}^2)}), rf = 0 \text{if} rf < 0$$

where, behavior = $a \cdot lw + b \cdot rw + c$ depends linearly, with the parameters a, b and c, on the left wing angle, lw, and the right wing angle, rw.

Supplementary Material

Refer to Web version on PubMed Central for supplementary material.

ACKNOWLEDGMENTS

We thank A. Nern for sharing flies and generous technical advice, B. Pfeiffer and G. Rubin for providing pJFRC64, pJFRC118, and pJFRC119 flies, and R. Harris for building fly lines, sharing preliminary results, and providing critical feedback in the use of fly reagents. We thank K. Hibbard, D. Hall, J. Kao and the Janelia Fly Core for fly crosses and support, E. Chiappe for initial anatomy experiments, M. Reiser and J. Truman for sharing equipment, J. Liu for technical support, V. Iyer for ScanImage support, T. Adelman for helpful suggestions, and L. Looger and the Janelia GENIE team for GCaMP5 and GCaMP6. We are grateful to A. Leonardo, M. Reiser, E. Chiappe, J. Freeman, A. Karpova, S. Huston and members of Vivek's lab for useful discussions and comments on the manuscript. This work was supported by the Howard Hughes Medical Institute.

REFERENCES

1. Bausenwein B, Muller NR, Heisenberg M. Behavior-dependent activity labeling in the central complex of Drosophila during controlled visual stimulation. J Comp Neurol. 1994; 340:255–268. [PubMed: 8201021]
2. Neuser K, Triphan T, Mronz M, Poeck B, Strauss R. Analysis of a spatial orientation memory in Drosophila. Nature. 2008; 453:1244–1247. [PubMed: 18509336]
3. Ofstad TA, Zuker CS, Reiser MB. Visual place learning in Drosophila melanogaster. Nature. 2011; 474:204–207. [PubMed: 21654803]
4. Liu G, et al. Distinct memory traces for two visual features in the Drosophila brain. Nature. 2006; 439:551–556. [PubMed: 16452971]
5. Pan YF, et al. Differential roles of the fan-shaped body and the ellipsoid body in Drosophila visual pattern memory. Learn Memory. 2009; 16:289–295.
6. Strauss R. The central complex and the genetic dissection of locomotor behaviour. Curr Opin Neurobiol. 2002; 12:633–638. [PubMed: 12490252]
7. Young JM, Armstrong JD. Structure of the adult central complex in Drosophila: Organization of distinct neuronal subsets. Journal of Comparative Neurology. 2010; 518:1500–1524. [PubMed: 20187142]
8. Hanesch U, Fischbach KF, Heisenberg M. Neuronal architecture of the central complex in Drosophila melanogaster. Cell Tissue Res. 1989; 257:343–366.
9. Renn SCP, et al. Genetic analysis of the Drosophila ellipsoid body neuropil: Organization and development of the central complex. Journal of Neurobiology. 1999; 41:189–207. [PubMed: 10512977]
10. Trager U, Wagner R, Bausenwein B, Homberg U. A novel type of microglomerular synaptic complex in the polarization vision pathway of the locust brain. Journal of Comparative Neurology. 2008; 506:288–300. [PubMed: 18022957]
11. Jenett A, et al. A GAL4-Driver Line Resource for Drosophila Neurobiology. Cell reports. 2012; 2:991–1001. [PubMed: 23063364]
12. Wang J, Zugates CT, Liang IH, Lee CHJ, Lee TM. Drosophila Dscam is required for divergent segregation of sister branches and suppresses ectopic bifurcation of axons. Neuron. 2002; 33:559–571. [PubMed: 11856530]
13. Bonin V, Histed MH, Yurgenson S, Reid RC. Local diversity and fine-scale organization of receptive fields in mouse visual cortex. J Neurosci. 2011; 31:18506–18521. [PubMed: 22171051]
14. Seelig JD, et al. Two-photon calcium imaging from head-fixed Drosophila during optomotor walking behavior. Nat Methods. 2010

15. Maimon G, Straw AD, Dickinson MH. Active flight increases the gain of visual motion processing in Drosophila. Nat Neurosci. 2010; 13:393–399. [PubMed: 20154683]
16. Chiappe ME, Seelig JD, Reiser MB, Jayaraman V. Walking modulates speed sensitivity in Drosophila motion vision. Curr Biol. 2010; 20:1470–1475. [PubMed: 20655222]
17. Heinze S, Reppert SM. Sun compass integration of skylight cues in migratory monarch butterflies. Neuron. 2011; 69:345–358. [PubMed: 21262471]
18. Heinze S, Homberg U. Maplike representation of celestial E-vector orientations in the brain of an insect. Science. 2007; 315:995–997. [PubMed: 17303756]
19. Rosner R, Homberg U. Widespread sensitivity to looming stimuli and small moving objects in the central complex of an insect brain. J Neurosci. 2013; 33:8122–8133. [PubMed: 23658153]
20. Guo P, Ritzmann RE. Neural activity in the central complex of the cockroach brain is linked to turning behaviors. J Exp Biol. 2013; 216:992–1002. [PubMed: 23197098]
21. Bahl A, Ammer G, Schilling T, Borst A. Object tracking in motion-blind flies. Nat Neurosci. 2013; 16:730–738. [PubMed: 23624513]
22. Poggio T, Reichard W. Theory of pattern induced flight orientation of fly Musca domestica. Kybernetik. 1973; 12:185–203. [PubMed: 4718020]
23. Hubel DH, Wiesel TN. Receptive fields, binocular interaction and functional architecture in the cat's visual cortex. J Physiol-London. 1962; 160 106-&.
24. Priebe NJ, Ferster D. Mechanisms of neuronal computation in mammalian visual cortex. Neuron. 2012; 75:194–208. [PubMed: 22841306]
25. Freifeld L, Clark DA, Schnitzer MJ, Horowitz MA, Clandinin TR. GABAergic lateral interactions tune the early stages of visual processing in Drosophila. Neuron. 2013; 78:1075–1089. [PubMed: 23791198]
26. Egelhaaf M, Borst A. A look into the cockpit of the fly: visual orientation, algorithms, and identified neurons. J Neurosci. 1993; 13:4563–4574. [PubMed: 8229185]
27. Pfeiffer K, Kinoshita M, Homberg U. Polarization-sensitive and light-sensitive neurons in two parallel pathways passing through the anterior optic tubercle in the locust brain. Journal of Neurophysiology. 2005; 94:3903–3915. [PubMed: 16049147]
28. Mu LY, Ito K, Bacon JP, Strausfeld NJ. Optic glomeruli and their inputs in Drosophila share an organizational ground pattern with the antennal lobes. Journal of Neuroscience. 2012; 32:6061–6071. [PubMed: 22553013]
29. Collett T. Visual neurones for tracking moving targets. Nature. 1971; 232:127–130. [PubMed: 4933247]
30. O'Carroll D. Feature-detecting neurons in dragonflies. Nature. 1993; 362:541–543.

ADDITONAL REFERENCES

31. Zhang YQ, Rodesch CK, Broadie K. Living synaptic vesicle marker: synaptotagmin-GFP. Genesis. 2002; 34:142–145. [PubMed: 12324970]
32. Pfeiffer BD, et al. Refinement of tools for targeted gene expression in Drosophila. Genetics. 2010; 186:735–755. [PubMed: 20697123]
33. Nicolai LJJ, et al. Genetically encoded dendritic marker sheds light on neuronal connectivity in Drosophila. Proc Natl Acad Sci U S A. 2010; 107:20553–20558. [PubMed: 21059961]
34. Pfeiffer BD, Truman JW, Rubin GM. Using translational enhancers to increase transgene expression in Drosophila. Proc Natl Acad Sci U S A. 2012; 109:6626–6631. [PubMed: 22493255]
35. Struhl G, Basler K. Organizing activity of wingless protein in Drosophila. Cell. 1993; 72:527–540. [PubMed: 8440019]
36. Peng H, et al. BrainAligner: 3D registration atlases of Drosophila brains. Nat Methods. 2011; 8:493–500. [PubMed: 21532582]
37. Weber F, Machens CK, Borst A. Spatiotemporal response properties of optic-flow processing neurons. Neuron. 2010; 67:629–642. [PubMed: 20797539]
38. Suver MP, Mamiya A, Dickinson MH. Octopamine neurons mediate flight-induced modulation of visual processing in Drosophila. Curr Biol. 2012

39. Pologruto TA, Sabatini BL, Svoboda K. ScanImage: flexible software for operating laser scanning microscopes. Biomed Eng Online. 2003; 2:13. [PubMed: 12801419]

40. Reiser MB, Dickinson MH. A modular display system for insect behavioral neuroscience. J Neurosci Methods. 2008; 167:127–139. [PubMed: 17854905]

41. Chichilnisky EJ. A simple white noise analysis of neuronal light responses. Network. 2001; 12:199–213. [PubMed: 11405422]

42. Niell CM, Stryker MP. Highly selective receptive fields in mouse visual cortex. J Neurosci. 2008; 28:7520–7536. [PubMed: 18650330]

43. Swindale NV. Orientation tuning curves: empirical description and estimation of parameters. Biological Cybernetics. 1998; 78:45–56. [PubMed: 9518026]

44. Swindale NV, Grinvald A, Shmuel A. The spatial pattern of response magnitude and selectivity for orientation and direction in cat visual cortex. Cerebral Cortex. 2003; 13:225–238. [PubMed: 12571113]

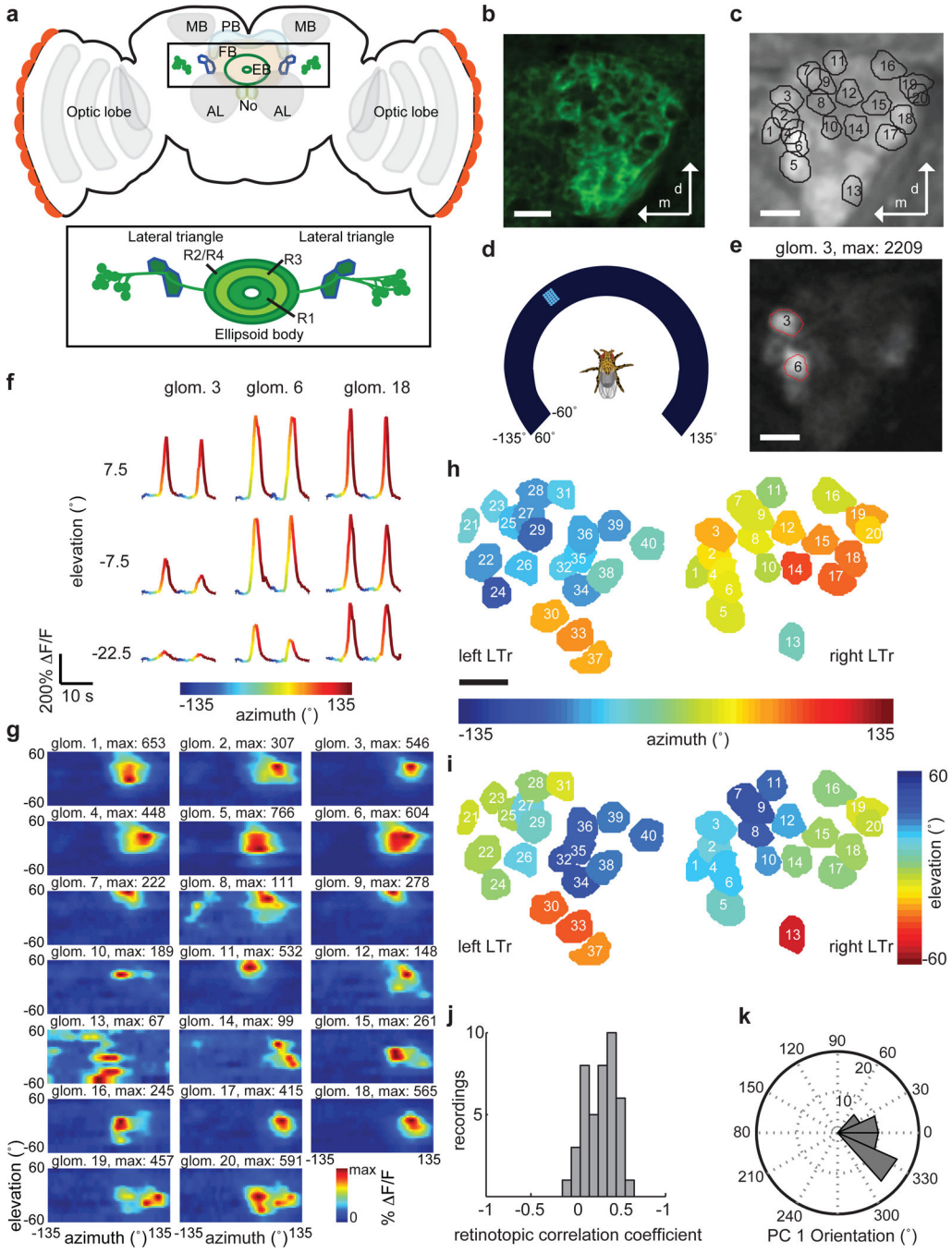

Figure 1. *Drosophila* ellipsoid body ring neurons arborize in visually responsive LTr microglomeruli that show a retinotopic organization

a, Schematic of fly central brain showing antennal lobe (AL), mushroom bodies calyces (MB) and optic lobes along with sub-structures of the central complex: ellipsoid body (EB), fan-shaped body (FB), protocerebral bridge (PB), and noduli (NO). Inset: EB ring neurons (R1–R4) and LTr. **b,** Frame of a confocal stack showing LTr microglomeruli labeled by pan-neuronal GFP expression. **c,** Projection of two-photon calcium imaging video of LTr with overlay of microglomeruli selected based on responses to moving visual stimuli. 20±5

microglomeruli delineated in individual planes of focus; 30±4 microglomeruli over multiple planes of focus (n = 11 flies) (see Methods). **d,** Schematic of RF mapping setup with fly positioned in center of curved visual display. **e,** Sample frame from trial showing responses in selected glomeruli (red outlines). **f,** Calcium transients of three LTr microglomeruli in response to visual stimulus moving left to right in front of the fly at different elevations. **g,** Two-dimensional response maps (two-trial averages) for all microglomeruli shown in **c**. **h,** LTr microglomeruli from left and right hemisphere of same fly, colored according to center of RF in azimuth, and **i,** elevation. **j,** Histogram of correlation coefficients between RF center and anatomical position. For n = 42 focal planes with 20±5 glomeruli, correlation is significantly different than for randomly arranged microglomeruli ($r = 0.27 \pm 0.17$, $p = 2.3 \cdot 10^{-17}$, n = 11 flies), indicating retinotopy in the organization of microglomeruli across flies. **k,** Histogram of primary retinotopic axis of LTr map as found by principal component analysis (see Methods, n = 42 focal planes, 11 flies). All scale bars: 5μm.

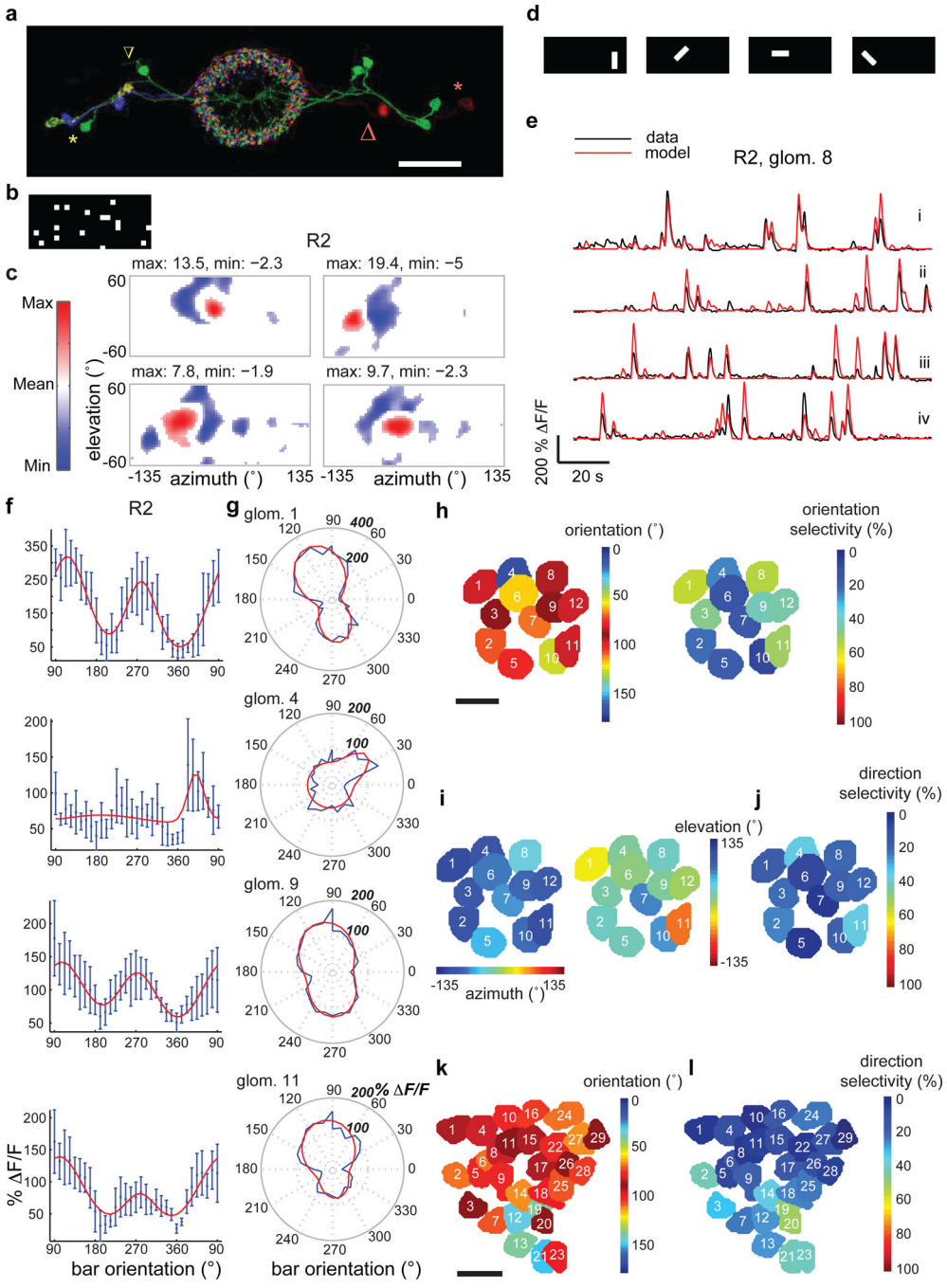

Figure 2. Ring neurons are tuned to specific visual features and orientations

a, Multicolor FLP-out of R2 neurons showing three cell bodies on each side along with their color-matched microglomeruli (green, light green and purple at left; two green and one red at right). Red and yellow stars mark two cell bodies (one on each side, lateral) and arrows of like color their respective LTr microglomeruli (medial). All neurons send processes throughout EB rings. Scale bar: 30μm. **b**, Example frame of white noise stimulus used for RF mapping using reverse correlation. **c**, Sample RFs of R2 microglomeruli. Red subfields: excitatory responses > 30% of maximum; blue subfields: inhibitory responses < 30% of

minimum of mean-subtracted weighted average. See Extended Data Fig. 8 for all RFs. **d**, Bright bars with four different orientations used as test features. **e**, Modeled and actual (black) ΔF/F changes of an R2 microglomerulus in response to differently oriented bars (fly 2 in Extended Data Fig. 7). In red: (i) trial used for fitting parameters, and, (ii)–(iv) tests. **f**, Orientation tuning curves for R2 neurons (two-trial average, fit in red). 90° corresponds to back-to-front movement of vertical bar, 270° to front-to-back movement of vertical bar. Error bars: standard deviation. **g**, Polar plots of orientation tuning data and fits (red) for data shown in **f**. **h**, Microglomeruli of R2 neurons colored by orientation preference (collapsed to 0°–180°) and orientation selectivity (two-trial average). **i**, Same microglomeruli as in **h** colored by azimuth and elevation of center of their excitatory RFs, measured using horizontally moving bars as described in Extended Data Fig. 1 (two-trial average). **j**, Direction selectivity of same microglomeruli (two-trial average). **k**, Preferred orientation (collapsed to 0°–180°) and **l**, direction selectivity of microglomeruli in pan-neuronal line (both four-trial average). See Methods for analysis details. Scale bar for **h–k**: 5μm.

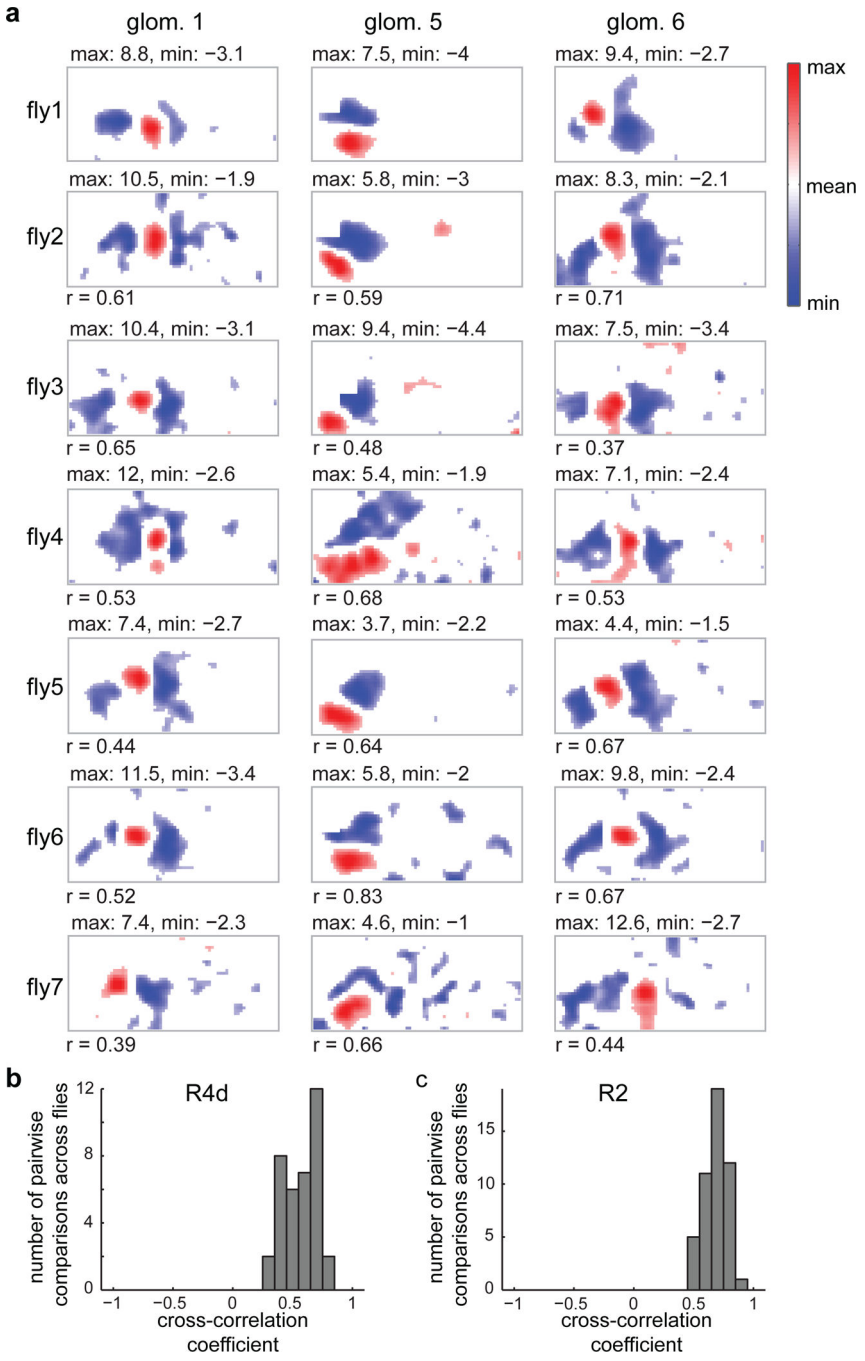

Figure 3. Ring neuron LTr microglomeruli show stereotyped RF properties across flies

a, Subset of RFs measured in R4d neurons across seven flies aligned by similarity (see Extended Data Fig. 8b for full set). Numbers below RFs are cross-correlations with top RF in column as template. **b**, Histogram of cross-correlation values calculated for R4d neuron RFs with best-matched template. **c**, Histogram of cross-correlation values for R2 neurons (n = 6 flies, see Extended Data Fig. 8a for RFs).

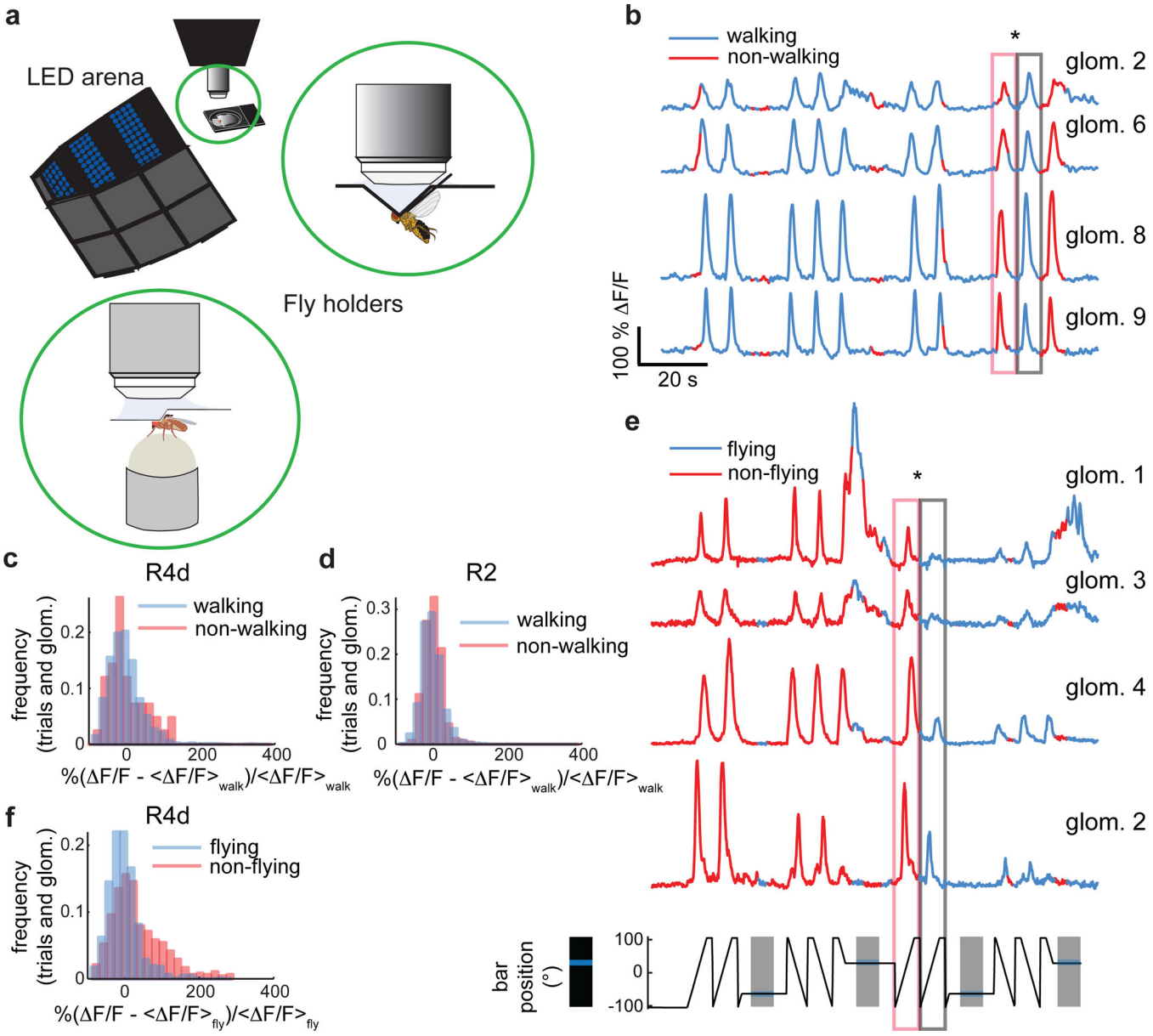

Figure 4. Ring neuron visual responses are not significantly modulated during walking but diminished during flight

a, Setup for two-photon imaging in behaving flies. Insets: Schematic of fly tethered in flying holder, and positioned on air-supported ball in walking holder. **b**, Subset of simultaneously recorded R2 neurons during walking. Starred boxes: responses to identical visual stimuli when fly is stationary versus walking. Azimuthal position of visual stimulus shown in **e** (bottom). **c**, Distributions of R4d neuron visual responses during walking and non-walking conditions are not significantly different (n = 14 flies, $trials_{walking}$ = 1722, $trials_{walking<50\%}$ = 42, $mean_{walking}$ = 0±44.3, $mean_{walking<50\%}$ = 1.1±49.7, p = 0.45). **d**, Same as **c** for R2 neurons (n = 8 flies, $trials_{walking}$ = 2015, $trials_{walking<50\%}$ = 245, $mean_{walking}$ = 0±28.1, $mean_{walking<50\%}$ = −2.2±24.4, p = 0.37). **e**, Subset of simultaneously recorded R4d microglomeruli during flight. Starred boxes: diminished responses to identical visual stimuli

during flight. **f**, Distributions of all R4d microglomeruli recorded shows significant shift towards lower responses during flight (n = 13 flies, $trials_{flying}$ = 759, $trials_{flying<50\%}$ = 481, $mean_{flying}$ = 0±42.2, $mean_{flying<50\%}$ = 31.2±72.3, $p = 6 \cdot 10^{-15}$). All p-values: two-sample Kolmogorov-Smirnov test.